Journal of Petroleum Exploration and Production Technology (2023) 13:2417–2436
https://doi.org/10.1007/s13202-023-01684-5

ORIGINAL PAPER-EXPLORATION ENGINEERING

Drilling-vibration response characteristics of rocks based on Hilbert–Huang transform

Xinxin Fang[1,2] · Hong Feng[2] · Yunhong Wang[2] · Xiao Liu[3] · Xiaoyu Liu[3] · Sihui Xu[3] · Yanqiu Wang[3] · Xiaowei Ni[3]

Received: 5 October 2022 / Accepted: 22 July 2023 / Published online: 2 August 2023

Abstract

Currently, there are no in-situ methods to quantify drilling-vibration response characteristics of different lithologies. Here, we quantified the vibration responses of four lithologies (limestone, sandstone, coal, and mudstone) using a combination of theoretical deduction and numerical simulation. First, a drilling-vibration model of a particular rock was established, and the differential equations of motion and vibration responses to rock/drill bit interactions with the formation were derived. Next, finite-element simulation was adopted to simulate the rock/drill-bit interactions of the four lithologies. Finally, the Hilbert–Huang transform (HHT) was applied to extract characteristic waveforms, frequency bands, peak frequencies, and marginal spectra of vibration signals. Simulations revealed that the highest and lowest vibration responses were observed in limestone and mudstone, respectively. Vibration acceleration was proportional to the Young's modulus of rocks, whereas vibration displacement and velocity were inversely proportional to Young's modulus, compressive strength, and density. Based on the HHT results, among the four lithologies, vibration responses had the largest characteristic frequency segments and peak frequencies in limestone (28.1–34.6 kHz and 33.4 kHz, respectively), whereas those of mudstone were the smallest (15.6–21.3 kHz and 19.6 kHz, respectively). The results of this study provide a theoretical basis for establishing an identification method and expert knowledge database of lithology based on drilling-vibration responses.

Keywords Drilling response · Vibration · Hilbert–Huang transform · ABAQUS · Lithology identification

List of symbols

A	Amplitude of simple harmonics (mm)
$a(t)$	Vibration acceleration of rock (m/s^2)
$a_k(t)$	Amplitude of the k-th order eigenmodal function $h_k(t)$ of the original signal (m/s^2)
c	Damping coefficient (Dimensionless)
D	Damage coefficient (Dimensionless)
$E\prime$	Macroscopic equivalent elastic modulus of rocks with cracks (GPa)
F	Impact vibration force (N)
F_0	Amplitude of the vibration response force of rock (N)
hi	New data sequence (Dimensionless)
IMF_j	Component obtained by EMD decomposition (Dimensionless)
k	Elastic coefficient (Dimensionless)
$q(t)$	Decomposition component (Dimensionless)
$S(x)$	Main function (mm)
SD	Standard deviation (Dimensionless)
R_n	Residual term of the mean trend of the signal (Dimensionless)
$v(t)$	Vibration velocity (m/s)
$w(t)$	Variation of vibration response force with time (rad/s)
$x(t)$	Vibration displacement (m)
ε	Strain (Dimensionless)
$\overline{\varepsilon_0}^{\mathrm{pl}}$	Critical plastic strain (Dimensionless)
θ_0	Time-independent constant representing the initial phase angle of displacement
σ_{y0}	Critical yield stress (MPa)
σ_x	Horizontal principal stresses in x axis directions (MPa)
σ_y	Horizontal principal stresses in y axis directions (MPa)
σ_z	Horizontal principal stresses in z axis directions (MPa)
σ_{yx}	Shear stresses on the normal yx stress plane (MPa)

✉ Xinxin Fang
fx15827573109@163.com

[1] China Coal Research Institute, Beijing, 100013, China

[2] Xi'an Research Institute of China Coal Technology & Engineering Group Corp, Xian, Shaanxi 710077, China

[3] Tarim Oilfield Company, Korla, Xinjiang 841000, China

σ_{zy} Shear stresses on the normal *zy* stress plane (MPa)
σ_{zx} Shear stresses on the normal *zx* stress plane (MPa)

Abbreviations

WOB Weight on bit
HHT Hilbert–Huang transform
IMF Intrinsic mode function
EMD Empirical mode decomposition
ANN Artificial neural network
PDC Polycrystalline diamond compact

Introduction

In petroleum, mining, and tunnel engineering applications, drilling operations are useful in establishing drilling parameters, adjusting drilling trajectory, determining mud density, and predicting geological accidents (Darwesh et al. 2020; Fang et al. 2022; Fang and Feng 2021; Zhu et al. 2023). During drilling, it is necessary to consider lithological data at the current position of the drill bit, assess the geological characteristics of the drilled formation, and identify the interface of the current rock stratum such that the type of bit, drilling method, and optimization of drilling parameters (e.g., rock-breaking efficiency and drilling cost) can be adapted to the rock characteristics (Ahmed et al. 2022; Sahoo and Jha 2017; Yue et al. 2022; Fang et al. 2023a, b). The prediction of rock properties via drilling parameters is an efficient and convenient method for obtaining data on formations that provide the advantages of timeliness, accuracy, environmental protection, and energy efficiency. Currently, drilling pressure, torque, drilling speed, and rotation speed are used to establish quantitative criteria for lithological discrimination (Lakshminarayana et al. 2020; Aydin and Hanifi 2021; Jeroen et al. 2021; Fang et al. 2023a, b). Nevertheless, studies have not yet investigated the prediction of lithology from the vibration responses to drill bit-rock interactions. These interactions cause the rock to break due to the energy released inside the rock in the form of vibrations. The internal vibration responses of rocks are indicative of their mechanical characteristics and contain a large amount of information on lithology and rock mechanics (Majeed et al. 2020; Utku et al. 2021; Bameri et al. 2021). Investigating the drilling-vibration response of rocks can thus provide theoretical support for developing new methods for identifying rock properties. To fill this knowledge gap, the present study aimed to comprehensively quantify drill bit-rock interaction characteristics, the vibration responses of rocks of four different lithologies (limestone, sandstone, coal, and mudstone), and their relationships with rock mechanics parameters.

Although the drilling-vibration characteristics of drill pipes and acoustic signals have received considerable attention, there exist few studies on the drilling-vibration responses of rocks with different lithologies. Rajesh et al. (2013) examined the relationship between acoustic signals and rock properties during drilling by predicting rock mechanics parameters, such as Young's modulus and uniaxial compressive strength, through extraction of acoustic signals during drilling. Vardhan et al. (2009) determined the degree of rock damage based on the sound level during drilling. Vijaya et al. (2019) calibrated the lithology by extracting the principal frequency of the noise signal during drilling, thereby establishing a quantitative relationship between lithology and acoustic signals. However, some limitations exist in assessing lithology and rock mechanics characteristics by analyzing acoustic signals from drilling, mainly owing to the relatively complex source of noise signals. Such signals are generated by not only the breaking of rock but also by the rotation of the drilling tools, fluid circulation, and the sound of the drilling rig in the hole. In addition, the evident dissipation effect of noise signals causes the energy to be easily lost, thereby making it challenging to accurately record these signals. Rajesh et al. (2011) investigated the relationship between drill pipe vibration and rock characteristics by estimating rock mechanics parameters, such as tensile strength and compressive strength of rocks, through the analysis of drill string-vibration signals from rotary drilling. Mehrbod and Raheb (2020) carried out a comprehensive analysis of noise and drill string-vibration signals to predict the mechanical characteristics of hard rocks. Kenneth et al. (2022) classified and evaluated drill string-vibration signals of percussion drilling and characterized rock characteristics via a machine-learning algorithm. Esmaeili et al. (2012) evaluated stratum classification based on the high-order frequency of drill string-vibration signals. Wang et al. (2022) established an identifying relationship between axial vibration and the lithology of a bottom hole by analyzing axial vibration characteristics of a drill string. Li et al. (2011) classified and evaluated drill string-vibration signals to predict variation in lithology near the drill bit. Liu et al. (2017) performed experiments to extract vibration signals of different media drilled by drill bits, established "fingerprint" characteristics of different signals, and ultimately characterized different materials via artificial neural networks. Although the relationship between drill string vibration and rock characteristics has been studied, interpretation has proven difficult because the vibration signal of the drill string contains not only rock information descriptive of rock drill bit interaction but also various types of noise, such as from fluid in the hole, drill string torsional vibration, and viscous slip vibration. To date, the identification of lithology through drill-string vibration has mostly been considered from a qualitative perspective.

Standard time–frequency conversion methods, such as Fourier and wavelet transforms, currently tend to be used to extract the characteristics of vibration signals. The Fourier transform is more suitable for analyzing vibration signals

with linear, stationary, and normal distribution characteristics but can easily generate false frequencies when nonlinear, non-stationary, and fluctuating signals are analyzed. In contrast, the Hilbert–Huang transform (HHT) first decomposes the signal into an intrinsic mode function (IMF) of different scales through empirical mode decomposition (EMD) based on instantaneous frequency; then, the IMF is transformed into a marginal spectrum with different energies via Hilbert spectrum analysis. Compared with the traditional signal-processing methods, HHT entirely eliminates the constraints of linearity and stationarity and allows a clear physical interpretation of the outcomes (Wang et al. 2022). The HHT can extract the time, frequency, and energy distribution characteristics of the signal and is adaptive enough for application to sudden signals and the extraction and analysis of unsteady signal characteristics, such as drilling vibrations. Therefore, it has been widely and successfully applied. Lee et al. (2010) combined HHT and wavelet transform to study the transient effect of composite materials subjected to high-speed impacts, to determine the structural firmness of the materials. Dushyanth et al. (2016) integrated HHT and a support vector machine to analyze vibration signals in component-damage detection. Wang et al. (2022) applied HHT to extract and analyze the vibration signal from the pneumatic breaking of dry ice powder, with the aim of assessing breaking and damage degree through this information channel. Diao et al. (2022) employed HHT to separate vibration components related to damage in structural damage detection. These studies mainly focused on the application of HHT to structural flaw detection, fault diagnosis, rock blasting, and fields instead of on feature extraction from drilling vibration. Therefore, the present study aimed to introduce HHT into the extraction and analysis of drilling-vibration responses of rocks with different lithologies.

We established a drilling-vibration model, derived a differential motion equation, and generated a vibration response equation for the bit-induced breaking of rock (Fig. 1). Based on numerical simulations of the bit-rock interactions using ABAQUS, the stress distribution characteristics of the rock surface and drilling-vibration responses in the form of velocity, acceleration, and displacement changes were quantified. The characteristic frequency band, peak frequency, and marginal spectrum of vibration signals of rocks with limestone, sandstone, coal, and mudstone lithologies were extracted using HHT, and a criterion for identifying lithology based on the vibration response frequency was established. This study establishes a theoretical foundation for identifying lithology and predicting rock mechanics parameters based on the drilling-vibration responses of rocks.

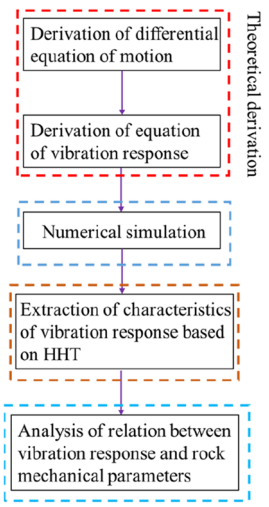

Fig. 1 Flowchart of the study structure

Methods

Mechanical model of drilling vibration

During the drilling operation, the bit-rock interaction causes a quick strain energy release as an elastic wave and later produces a corresponding vibration inside the rock. The bit-rock interaction was simplified as the action between a flat-bottomed indenter and the rock, and a vibration model of the rock was established by applying multiple spring superpositions to simulate the flat-bottomed head, as shown in Fig. 2. Ignoring the coupling force between the springs, the region under the indenter is divided infinitely.

Derivation of differential motion equation of rock under drilling vibration

As the action force between the flat-bottomed indenter and the rock medium surface is the same at each point on the rock, the action of the entire head and rock medium can be represented by considering the interaction between one point on the flat-bottom head and a micro-element on the rock medium plane. Therefore, a single micro-element was separately extracted for analysis. The dynamic vibration model of rock micro-elements was simplified into a simple harmonic

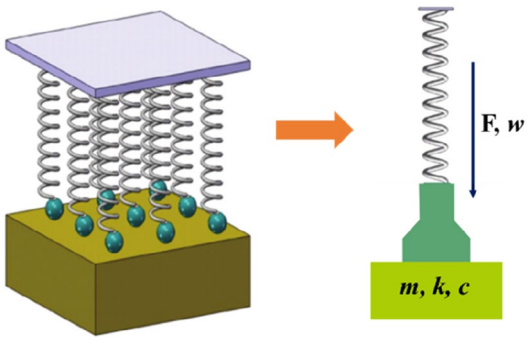

Fig. 2 Simplified model of a bit-rock interaction

model, as shown in Fig. 2. This simplified drilling model was a drilling-vibration system composed of a drill bit and a rock. The rock was regarded as an elastic body, neglecting the influence of small lateral vibrations of the drilling equipment and of air resistance. Under ideal conditions, vibration produced by rock represents a single-degree-of-freedom forced vibration under an impact load. The impact vibration force is F, the elastic coefficient is k, and the damping coefficient is $\boldsymbol{c}$. Considering that the impact exerted by a drilling bottom hole assembly is significantly greater than the weight imposed on the bit during the drilling operation, the effect of the drilling tool weight on the rock could be ignored.

In the model shown in Fig. 3, the rock interacts with the bit to produce a simple harmonic vibration. Using Newton's second law of motion, the stress of the rock micro-element under a simple harmonic motion can be described as follows:

$$m\frac{\partial^2 s}{\partial t^2}+\frac{\partial^2}{\partial x^2}\left[k\frac{\partial^2 s}{\partial x^2}+F\right]=0 \tag{1}$$

where $\partial^2\left[k\partial^2 s/\left(\partial x^2\right)\right]/\left(\partial x^2\right)$ is the load on the rock micro-element owing to vibrational deformation; k is the stiffness coefficient of the rock; $m\partial^2 s/\partial t^2$ is the mass inertia of the rock; m is the mass of the rock; and F is the vibration response force of the rock. $F=F_0 w(\mathrm{t})$, where F_0 is the amplitude of F, and w(t) is the variation of the vibration response force with time.

If the vibration of the rock is simplified as a simple harmonic motion, then according to the simple harmonic motion equation, assuming $s(x,t)=S(x)\sin(ft+x)$, where $S(x)$ is the main function, substituting $s(x,\ t)$ into Eq. (1) yields the following:

$$k\frac{\partial^2}{\partial x^2}\left(\frac{\partial^2 S}{\partial x^2}\right)+\frac{\partial^2 S}{\partial x^2}F_0 w(t)-\rho f^2 SA=0 \tag{2}$$

where A is the amplitude of the simple harmonic wave, and $S(x)$ is the main function.

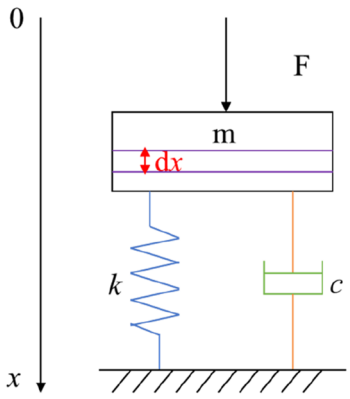

Fig. 3 Simple harmonic vibration mechanical model of rock micro-elements

The displacement of the rock micro-element at the initial position is zero, that is, $x=0, S(0)=0, S''(0)=0$. When the vibration displacement of the rock reaches its maximum, that is, $x=L, S(L)=0, S''(L)=0$, the motion equation of the vibration response force $\boldsymbol{F}$ of the rock can be derived as follows:

$$F(t)=ma(t)+cv(t)+kx(t) \tag{3}$$

where $a(t)$ is the vibration acceleration of the rock (m/s^2); c is the damping coefficient; v(t) is the vibration velocity (m/s); and $x(t)$ is the vibration displacement (m).

$$v(t)=\dot{x}=x'(t)=\frac{\mathrm{d}x(t)}{\mathrm{d}t} \tag{4}$$

$$a(t)=\frac{\mathrm{d}v(t)}{\mathrm{d}t}=\frac{\mathrm{d}^2x(t)}{\mathrm{d}t^2}=x''(t) \tag{5}$$

Therefore, Eq. (3) can be written as follows:

$$F(t)=m\ddot{x}+c\dot{x}+kx \tag{6}$$

Derivation of drilling-vibration response equation of rock

The impact force when the rock contacts the drill bit is assumed to be a simple harmonic excitation, and the vibration response force can be expressed as follows:

$$F(t)=kA\cos(wt) \tag{7}$$

where w is the vibration frequency of the simple harmonics.

The dimensionless constant ξ, representing the relative damping coefficient, was introduced by assuming $\xi=c/\left(2mw_0\right)$, where w_0 is the natural frequency of the rock. Combining Eq. (3) and (7) as well as substituting ξ into both equations yields the following vibration equation of rock, after simplification:

$$x''(t)+2\xi w0x'(t)+w_0^2x=w_0^2A\cos(wt) \tag{8}$$

Equation (8) is a second-order inhomogeneous linear differential equation with constant coefficients. By solving the differential, the special solution of Eq. (8) can be obtained as in Eq. (9):

$$x=F_0\cos\left(w_0t-\theta_0\right) \tag{9}$$

where x is the displacement of the rock under vibration, and θ_0 is the time-independent constant representing the initial phase angle of displacement. The general solution of Eq. (8) can be obtained as follows:

$$x=\frac{A}{w_0^2-w^2}\cos\left(wt+\theta\right)+F_0\cos\left(w_0t-\theta_0\right) \tag{10}$$

Equation (10) is the response equation of the vibration displacement of the rock under the action of the bit. The response equations for vibration velocity and acceleration can be derived by taking the respective derivatives.

Principles of empirical mode decomposition (EMD)

Empirical mode decomposition (EMD) is essentially a screening process. An instantaneous equilibrium point is obtained based on the mean values of the upper and lower fitted envelopes of a signal, and the IMF is calculated. To be capable of obtaining an IMF, two necessary conditions must be met: (1) the number of extreme points (maximum or minimum) of the signal should be consistent with the number of zero crossings or differ by no more than one unit; and (2) at any time, the sum of the value on the upper envelope formed by the local maximum and the value on the lower envelope formed by the local minimum should be zero; that is, the upper and lower envelopes should be symmetrical with respect to the time axis. As it is difficult to satisfy these two conditions, Huang proposed two assumptions: (1) all unstable random signals are composed of several independent IMF unit components; and (2) IMF components can be linear or discrete. Based on these assumptions, we performed EMD of the random vibration signal $x(t)$ by following the steps below:

1. Maxima and minima were determined for all t of signal $x(t)$.
2. Upper and lower envelopes were obtained by fitting all maxima and minima with a cubic spline interpolation function.
3. The average value of all upper and the lower envelope limits was calculated and denoted m_1.
4. A new data sequence h_1 was constructed from the original signal x(t) and m_1 as follows:

$$h_1 = x(t) - m_1 \tag{11}$$

5. It was determined whether h_1 met the necessary conditions of IMF, that is, whether a negative local maximum or positive local minima existed. If so, h_1 was not an IMF, and the screening operation was still required. The specific iterative process was as follows: h_1 was treated as the original signal, and steps 1–4 were repeated, thus finally achieving h_2, h_3, h_4…

$$h_{k+1} : h_{k+1} = h_k - m_k \tag{12}$$

where $k \geq 1$, and m_k is the mean value of the upper and lower envelopes of h_k.

Once the condition of IMF was met using the above steps, and considering h_k as IMF1, the following steps were performed sequentially.

6) IMF1 was subtracted from the original signal $x(t)$ to obtain a new sequence $y(t)$ as follows:

$$y(t) = x(t) - \text{IMF1} \tag{13}$$

With $y(t)$ as the new original signal, step (1) was iterated to obtain a new IMF until the remaining signal was a monotonous or constant sequence and could not be decomposed further. The entire screening process was then completed. The decomposition of EMD can be expressed as follows:

$$x(t) = \sum_{K=1}^{n} \text{IMF}_j + R_n \tag{14}$$

where R_n is the residual term of the mean trend of the signal, and IMF_j is the component obtained by the EMD decomposition.

EMD was used to verify that any original signal consisted of multiple IMF components and residuals. The entire process resembled a screening operation in that IMF was extracted step-by-step from the original signal, in the order from small to large, according to the time characteristics. The end condition of the entire process was determined based on the standard deviation (SD) of two adjacent consecutive signal sequences. The precision of SD was determined based on actual requirements as follows:

$$\text{SD} = \sum_{k=1}^{n} \frac{\left(h_k - h_{k-1}\right)^2}{h_k^2} \tag{15}$$

The detailed implementation is illustrated in Fig. 4.

The principle of Hilbert transform

Based on the IMF component obtained via EMD, the Hilbert transform (HT) was performed to obtain the Hilbert spectrum, which can reflect the variation characteristics of the spectrum of a signal over time. For signal $x(t)$, the HT transform is expressed as follows:

$$y(t) = \frac{1}{\pi} \int \frac{x(\tau)}{t - \tau} \mathrm{d}\tau \tag{16}$$

The following equation is presented:

$$q(t) = x(t) + iy(t) \tag{17}$$

where q(t) is the decomposition component of x(t) and can be expressed as follows:

$$q(t) = g(t)e^{i\theta(t)} \tag{18}$$

where $g(t) = \sqrt{x^2(t) + y^2(t)}$,$\theta(t) = \arctan\left(\frac{y(t)}{x(t)}\right)$. The instantaneous frequency can be calculated as follows:

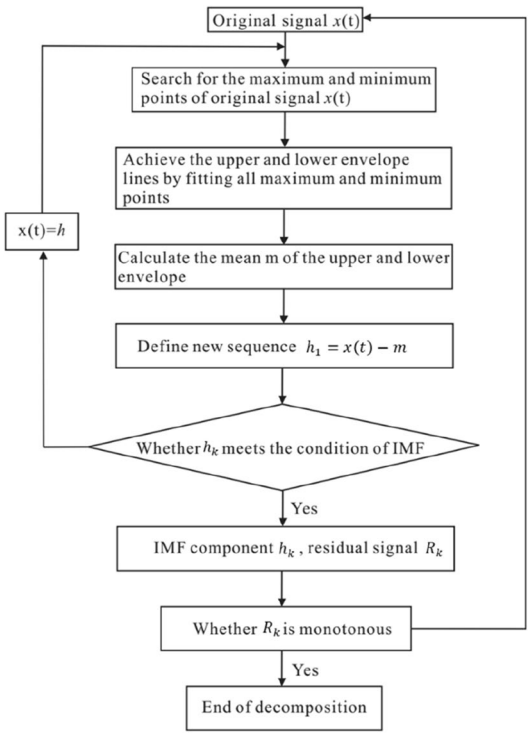

Fig. 4 Entire process of the EMD decomposition

$$f(t) = \frac{d\theta(t)}{dt} \tag{19}$$

Equation (19) indicates that the instantaneous frequency f(t) is a function of time.

The Hilbert transform was performed for all IMF components of x(t). The corresponding transformation expression can be obtained as follows:

$$H(t) = \sum_{k=1}^{n} a_k(t) e^{i \int w_j(t) \mathrm{d}t} \tag{20}$$

where $a_k(t)$ is the amplitude of the k-th order eigenmodal function $h_k(t)$ of the original signal $x(t)$.

After Fourier expansion, $H(t)$ can be written as follows:

$$H(w,t) = \mathrm{Re} \sum_{k=1}^{n} a_k(t) e^{i \int w_j(t) \mathrm{d}t} \tag{21}$$

The Hilbert marginal spectrum can be obtained by further integrating H (w, t):

$$H(w) = \int_0^T H(w,t) \mathrm{d}t \tag{22}$$

The obtained marginal spectrum characterizes the magnitude of the cumulative total amplitude of the signal within the entire time range. The accumulated total energy in the entire time domain can be estimated by integrating the square of H (w, t), that is the Hilbert energy spectrum, as follows:

$$H(w) = \int_0^T H^2(w,t) \mathrm{d}t \tag{23}$$

Numerical simulation of drilling vibration

Basic assumptions

To further understand the vibration response to the bit-rock interaction, the drilling process was simulated via ABAQUS finite-element software (Dassault Systèmes, Vélizy-Villacoublay, France). The numerical model comprised bits and rocks that conformed to the actual drilling process. With the aim of effectively quantifying the vibration responses of the rocks and considering the complexity of geological conditions during actual drilling, the drilling-vibration model included the following assumptions: (1) rocks are isotropic elastic materials, and primary fissures are not considered; (2) as the strength and hardness of the drill bit are significantly greater than those of the rock during the rock-breaking process, the bit is assumed to be a rigid body and any deformation is neglected; and (3) rock cuttings during drilling exert no impact on the drilling process.

Criterion for rock failure

The Hill yield function in ABAQUS was used to characterize the mechanical behaviors of the rocks during drilling, as shown in Eq. (24):

$$\left[F\left(\sigma_y - \sigma_z\right)^2 + G\left(\sigma_z - \sigma_x\right)^2 + H\left(\sigma_x - \sigma_y\right)^2 + L\sigma_{yx}^2 + M\sigma_{zx}^2 + N\sigma_{zy}^2\right]^{1/2} - \left(U\sigma_x + V\sigma_y + W\sigma_z\right) = 0 \tag{24}$$

where F, G, H, L, M, N, U, V, and W are material constants; σ_x,σ_y, and σ_z are horizontal principal stresses in the x, y, and z-axis dimensions, respectively; and σ_{yx},σ_{zy}, and σ_{zx} are shear stresses on the three normal stress planes yx, zy, and zx, respectively.

The yield function can be used to derive the rock stress and its corresponding equivalent plastic strain under the combined action of the drilling bit, as well as the *in-situ* stress given a specific drilling rate and weight on the bit. When the plastic strain reaches a certain value, the rock begins to disintegrate and then, fails to spall from the rock body. In this study, plastic strain was used as the basis for assessing rock failure:

$$\overline{\varepsilon}_0^{\mathrm{pl}} \le \varepsilon^p \le \overline{\varepsilon}_f^{\mathrm{pl}} \tag{25}$$

where $\overline{\varepsilon}_f^{\mathrm{pl}}$ is the equivalent plastic strain at complete rock failure; ε^p is the plastic strain; and $\overline{\varepsilon}_0^{\mathrm{pl}}$ is critical plastic strain.

The variation in the elastic modulus is generally applied to characterize the damage condition of the rock as follows:

$$D = 1 - \frac{E'}{E} = \begin{cases} 0 \left(\varepsilon \le \overline{\varepsilon}_0^{pl}\right) \\ 1 - \frac{\sigma}{\overline{\sigma}} \left(\varepsilon > \overline{\varepsilon}_0^{pl}\right) \end{cases} \tag{26}$$

where E is the elastic modulus of undamaged rock; E' is the macroscopic equivalent elastic modulus of rock with cracks; ε is strain; σ is stress; $\overline{\varepsilon}_0^{\mathrm{pl}}$ is critical plastic strain; D is the damage factor; and $\overline{\sigma}$ is the stress value of the curve (Fig. 5).

Figure 5 shows the relationship between the strain and stress during rock breakage. σ_{y0} and $\overline{\varepsilon}_0^{\mathrm{pl}}$ are the critical yield stress and critical plastic strain, respectively, at the beginning of the rock failure, where $D=0$; and $\overline{\varepsilon}_f^{\mathrm{pl}}$ is the equivalent plastic strain at complete rock failure, where $D=1$. When $D=1$, the rock fails completely and flakes off (Fig. 5).

Establishment of the model

A finite-element numerical model of the bit-rock interaction was established based on both the rock and elastic mechanics. The process of rock-breaking by the drill bit was simulated without considering the constraints of the complex stresses in the formation, as shown in Fig. 6. The model settings are listed in Table 1. The following boundary conditions were set: (1) the drill bit itself was not affected by any external force, and only the loads of static deadweight and dynamic impact existed in the vertical direction; and (2) the displacement constraint was applied to the rock bottom without considering the self-weight influence of the overlying rock. The contact settings were as follows: the drill bit type was a six-blade

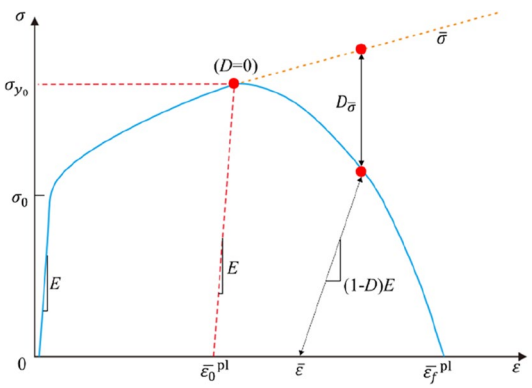

Fig. 5 Stress–strain curve during the entire failure process

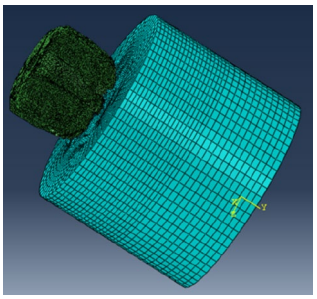

Fig. 6 Finite-element model of the bit-rock interaction

polycrystalline diamond compact (PDC) bit, with nine teeth on each blade, resulting in 54 contact surfaces between drill bit and rock. To improve the model accuracy, the rock grid was defined as a dense mesh element in the middle with a coarser surrounding mesh, and the mesh of the cutting teeth and the part of the bit in contact with the rock were densified. There were 96,608 nodes in the entire model, of which 71,025 were in the rock. With respect to load settings, an axial drilling load and a constant rotational speed were applied to the drill bit such that the drill bit could produce an axial impact and a rotary cutting action on the rock, thereby causing the rock to break. Rock and drilling parameter values are listed in Tables 2 and 3, respectively.

According to the above settings, the rock was defined as a flexible body, whereas the drill bit was defined as a rigid body. The drill teeth contacted and invaded the rock, with the axial impact of the drill bit breaking the rock, simulating the rock-breaking and drilling process. The Drucker–Prager criterion was selected as the rock-failure criterion (Liu et al. 2016).

Results

Analysis of numerical simulation of drilling-vibration

Stress distribution characteristics during drilling of rocks with four lithologies

During the numerical simulation of rock-breaking by drilling, an axial drilling force (weight on bit; WOB) as well as a rotational force along the axis was applied to the bit, which pushed the bit further into the formation. A PDC bit geometry was adopted for the numerical simulation, which mainly deformed the rock by cutting. The cutting edge on the bit cut into the

Table 1 Settings of the geometric model

Bit type	Bit size	Rock size
PDC	ϕ 215.9 mm	ϕ 400×200 mm

Table 2 Settings of the petrophysical parameters (Liu et al. 2020; Zhu et al. 2014)

Number	Lithology	Uniaxial compressive strength (Mpa)	Density (g cm^{-3})	Tensile strength (Mpa)	Elastic modulus (Mpa)	Poisson's ratio
1	Limestone	118.5	2.88	21.5	76.80	0.16
2	Sandstone	67.6	2.67	15.1	43.20	0.31
3	Coal	20.3	1.92	8.6	9.60	0.46
4	Mudstone	36.7	2.53	10.3	30.10	0.37

Table 3 Settings of the drilling parameters

Weight of bit/kN	RPM	Impact frequency (Hz)
22	250	100

rock under the action of WOB and the rotary force caused the shear failure of the rock. Three ways to disintegrate rock through drilling are currently in use: cutting, stamping, and grinding. Cutting is mainly carried out via axial drilling pressure and the rotary drive of the bit causes breakage. Stamping of rock is performed by the action of the axial load of the drilling rig to break the rock. The grinding process is performed by selecting a material with good wear resistance to break the rock under the drive of a certain force and rotation rate. In the process of the drill bit-rock interaction, when the stress of the rock exceeded its yield stress (σ_0), the rock reached the stage of plastic hardening, and the rock itself was not damaged. When the bit cutters continued to act on the rock, the stress of the rock exceeded the critical value of the yield stress (σ_{y0}) and the corresponding critical value of the plastic strain ($\overline{\varepsilon_0}^{\mathrm{pl}}$). Simultaneously, the rock reached the stress-softening stage, and the corresponding rock damage factor (D) continued to increase. As the equivalent plastic strain value approached $\overline{\varepsilon_f}^{\mathrm{pl}}$, the corresponding D value became 1. Subsequently, the rock reached a state of failure, and holes were formed.

Figure 7a–d shows the hole bottom shape formed by the bit-rock interaction at four time points. The hole bottom exhibited an uneven shape, which continuously changed under the ongoing action of bit and rock. The contact mode between drill teeth and rock showed an alternate cutting model, which indicated that the bit exerted a significant cutting effect on the rock.

Figure 8a–d shows the stress distribution nephogram generated by the bit-rock interaction in the four lithologies and reflects the variations in stress characteristics under the stamping and cutting of the bit. As shown in Fig. 8a–d, the stress concentration occurred when the rocks interacted with the bit; however, the concentration range and degree and consequently the reaction force of the rock on the bit, differed by lithology, as did the vibration responses of the bit and drill string to the reaction force. The stress concentration degree of limestone was the strongest, followed by sandstone, whereas those of coal and mudstone were relatively small (Fig. 8). This was mainly because the high strength and hardness of limestone resulted in the maximum energy accumulation in the interaction with the drill bit, as shown in the form of the stress distribution. The strength and hardness of coal and mudstone did not exceed those of limestone and sandstone, and their Young's modulus was smaller than those of these two lithologies. The relatively small instantaneous energy concentration in the interaction with the drill bit resulted in a weaker stress concentration distribution of coal and mudstone than that of limestone and sandstone.

Figure 9 indicates that the stress distributions of the four lithologies during the drilling operation differed from one another. The peak value of rock stress appeared at different times under the four lithologies, and the variation range of stress differed owing to the different mechanical rock properties. However, variations over time were similar to some extent. The stress on the rock surface fluctuated with time, and the distribution of this fluctuation mainly depended on the bit-rock interaction.

The rock-breaking of the bit exerted a certain impact on the rock, and the rock in return produced an equal reaction force on the bit. This was followed by the bit instantaneously breaking contact from the rock, thereby causing the stress on the rock surface to decrease from a peak to a valley. With the continuous advancement of the drilling process, the stress on the rock surface increased from a valley to a peak. This transformation process was similar to a periodic change process. Average stress within the same period for the four lithologies followed a descending order of limestone > sandstone > coal > mudstone (Fig. 9).

Vibration acceleration of the four lithologies

Under the bit-rock interaction, the rocks showed different internal vibration responses in the x, y, and z directions. Figure 10 shows the variation in the vibration acceleration with time in the x, y, and z directions for the four lithologies, following Eq. (5). The acceleration at the beginning of contact between bit and rock was relatively small, then accelerated under the progress of drilling in the descending order of limestone > sandstone > coal > mudstone.

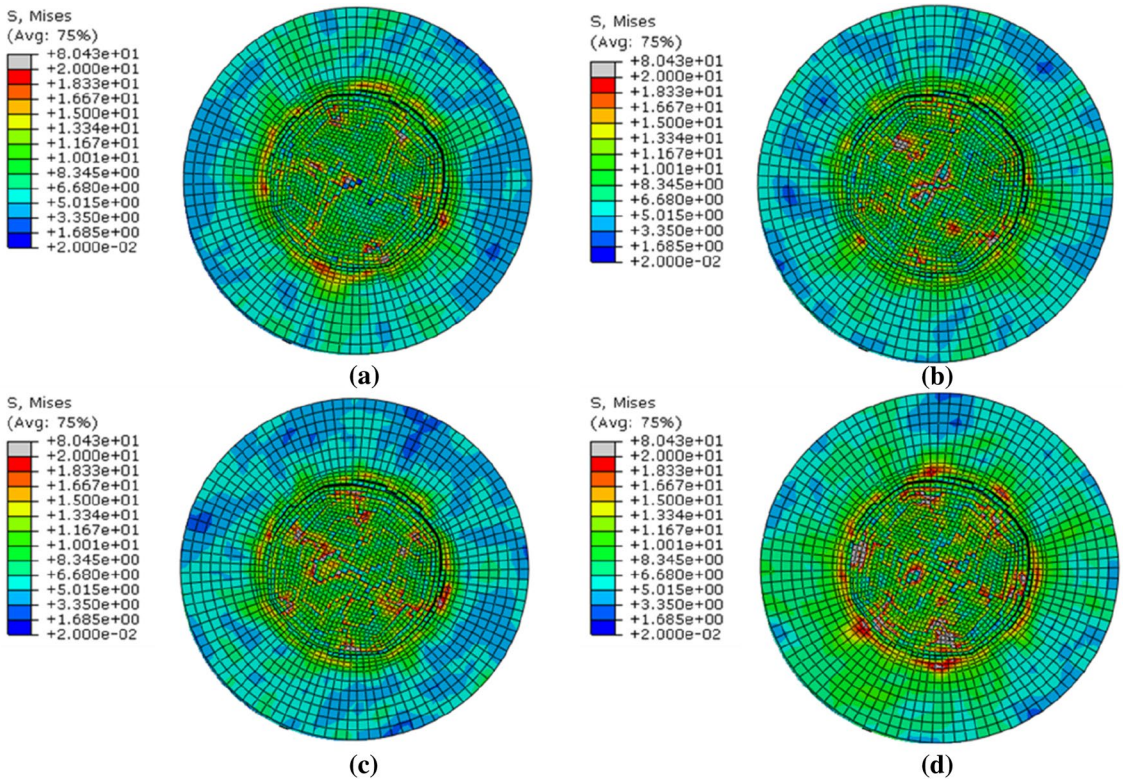

Fig. 7 Morphology of rock at the hole bottom at the four time points (t). **a** $t=1.0$ s and D = 0.82; **b** $t=2.0$ s and D = 0.86; **c** $t=3.0$ s and D = 0.95; and **d** $t=5.0$ s and D = 1.0

Acceleration in the direction of y (longitudinal acceleration) was significantly greater than that in the other directions (x and z).

Vibration displacement and vibration velocity of the four lithologies

Figure 11 illustrates the vibration displacement distribution of rocks with the four lithologies under the same WOB and rotation speeds. The vibration displacement of coal was the largest, and the vibration effect was the most notable. The entire rock showed a vibration response with different degrees of intensity, and the vibration effect from contact with the bit was the most substantial component. In contrast, the vibration effect of limestone was the least notable. Figure 12 shows that the vibration inside the rock gradually increased with the continuous progress of drilling. The vibration velocity difference (Eq. 10) between the four lithologies was initially small, then at later stages reached the highest values in coal, whereas vibration speed and frequency were the lowest in limestone. Vibration velocity (Eq. 4) among the four lithologies thus followed a descending order of coal > mudstone > sandstone > limestone (Fig. 13).

Analysis of vibration characteristics based on HHT

Previous studies have indicated that the longitudinal vibration produced by bit-rock interaction contains abundant information about the rock (Guo and Ma 2016). Therefore, the longitudinal vibration acceleration of the rocks with the four lithologies was extracted from the results of the ABAQUS-based simulations to determine their vibration characteristics. The EMD decomposition of the vibration acceleration information was performed with the help of the HHT toolbox of MATLAB software (MATLABS, Natick, MA, USA), and IMF and residual components were obtained. Each IMF component contained the corresponding vibration characteristics, as shown in Figs. 14, 15, 16 and 17. Based on the results of the EMD decomposition, the original signals of the four lithologies could be divided into 10 IMF components and one residual component. The vibration frequency and amplitude of the first component (IMF1) were the highest, reflecting the substantial amount of high-frequency vibrations. The vibration form preserved the main vibration characteristics of the original signal. The frequency of vibration of the IMF2–4 components was lower than that of the IMF1 component; the amplitude of vibration also declined but remained at medium–high levels, which preserved the partial vibration characteristics

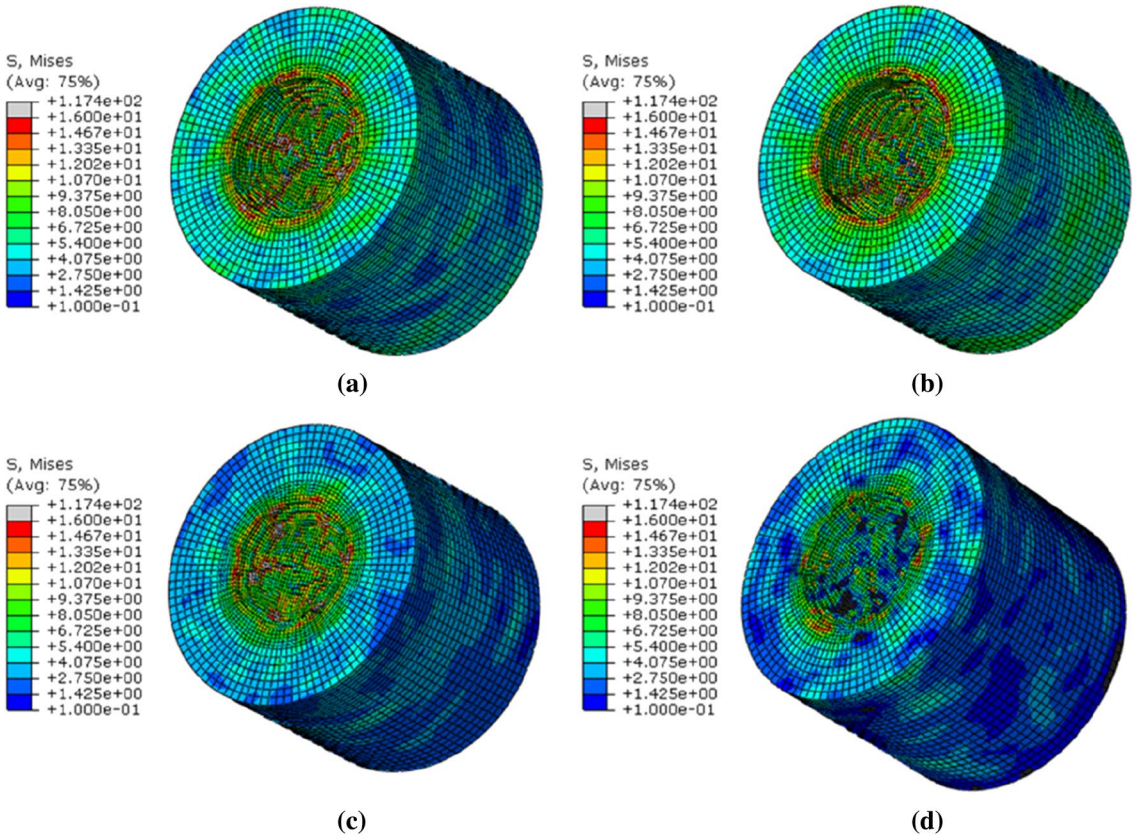

Fig. 8 Stress distributions in the rocks with the four lithologies for the same time $t = 1.0$ s: **a** limestone; **b** sandstone; **c** coal; and **d** mudstone

of the original signal. The IMF5–6 components notably decreased in vibration frequency and amplitude compared to IMF1–4, preserving barely a small portion of the vibration characteristics of the original signal. From IMF7 onwards, a low frequency was present, and the amplitude of the vibration decreased substantially. These parts of the vibration signal and residual component were ignored. The energy and kurtosis values of the IMF components were calculated. To facilitate comparisons, these two parameters were normalized; then, the kurtosis and distribution characteristics of the IMF components of the four lithologies were determined (Fig. 19). The kurtosis value characterizes the vibration signal distribution, with higher values indicating stronger vibration information. As shown in Figs. 18 and 19, the energy of the vibration signal was mainly concentrated in the IMF1–6 components, whereas from IMF7 onwards, the vibration energy and kurtosis value decreased considerably, even reaching zero. This distribution trend corresponded to the EMD decomposition results. It can therefore be concluded that the vibration characteristics of limestone, sandstone, mudstone, and coal were mainly reflected in the IMF1–6 components and that these IMF stages could be used to characterize the vibration characteristics of these four lithologies.

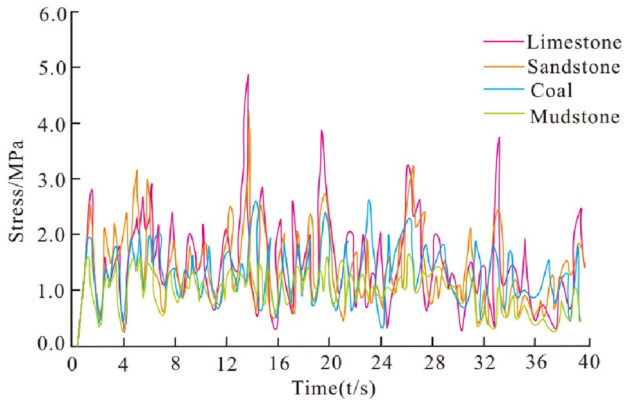

Fig. 9 Variation of rock stress with time among the four lithologies

IMF 1–6 was transformed via HT to obtain their analytical signals, and their instantaneous frequencies were determined. In this manner, the time-domain signals were converted to the frequency domain signals for analysis and processing. The HT spectrum of each IMF component was integrated in the time domain, and the corresponding marginal spectrum was accumulated to obtain the Hilbert distribution spectrum reflecting the variation in the frequency and

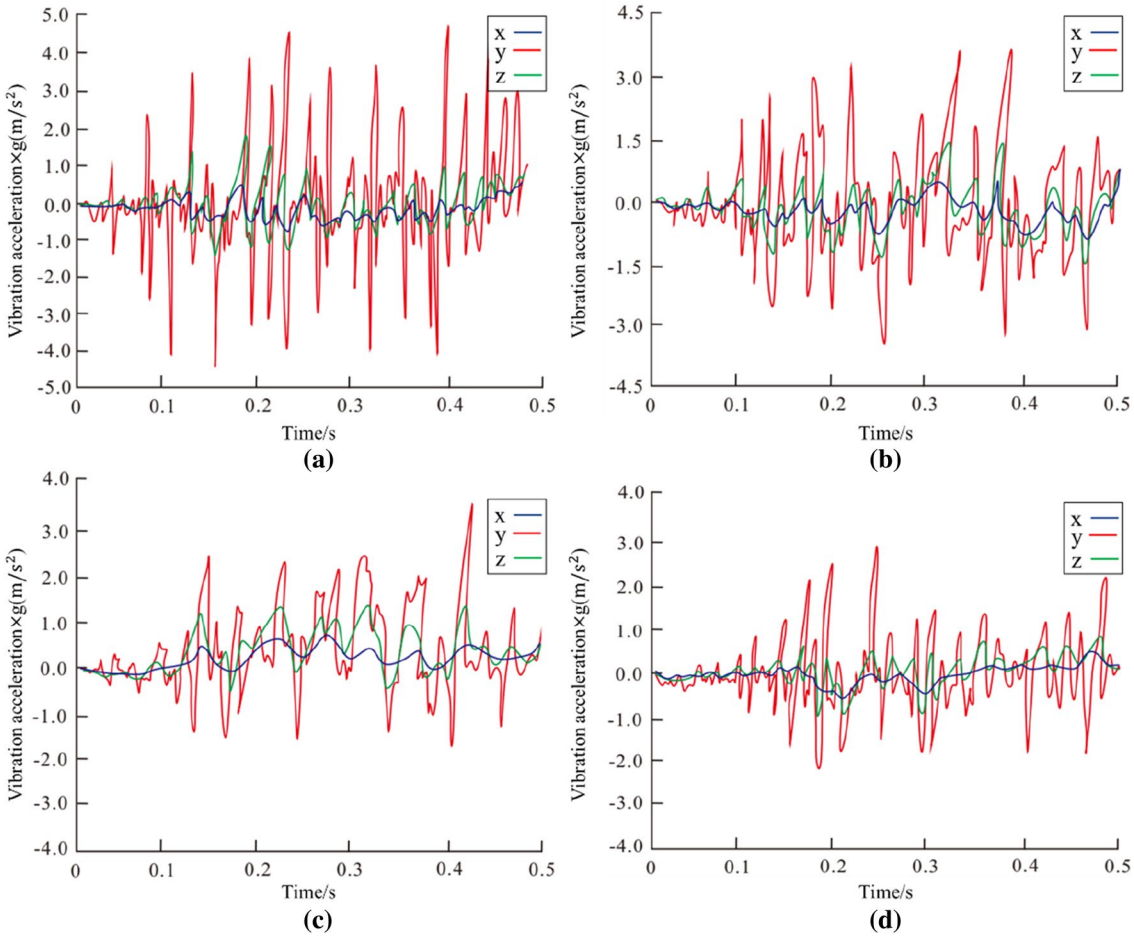

Fig. 10 Variation curves of the vibration acceleration in the directions of *x*, *y*, and *z* with time for rocks of the four lithologies: **a** limestone; **b** sandstone; **c** coal; and **d** mudstone

amplitude distributions of the respective lithology (Fig. 20). This spectrum could thus be used to establish the relationship between the lithology and the vibration frequency. Figure 20 indicates that each lithology had a corresponding frequency-concentration section, that is, a characteristic main frequency band and peak frequency. The peak frequencies of each lithology portrayed visible differences. The characteristic main frequency bands of limestone, sandstone, coal, and mudstone were estimated at 15.6–21.3, 20.5–26.3, 23.6–30.3, and 28.1–34.6 kHz, with corresponding peak frequencies of 19.6, 23.9, 28.8, and 33.4 kHz, respectively (Table 4).

The numerical simulation and HHT results indicate that large difference in vibration velocity, acceleration, and frequency exist among different lithologies. These results therefore allow establishment of a lithological identification method based on rock vibration characteristics, thereby facilitating the prediction of lithology during drilling, furthering the theoretical background for preventing geological disasters based on the drilling parameters, and allowing for early warning and assessment of rock drillability and surrounding rock stability.

Discussion and analysis of drivers of rock vibration responses

We used ABAQUS software to simulate the influences of rock mechanics parameters (uniaxial compressive strength, density, and Young's modulus) on rock drilling-vibration responses. We employed a control variable approach in which all but one factor were kept constant, while the effects of changes in the remaining factor were investigated. In this process, the drilling parameters of WOB, rotation speed, and drilling speed were kept constant, while the vibration response was extracted for analysis. Finally, the vibration response patterns of the numerical simulation were compared with the parameters tested in the laboratory to verify the simulated vibration response characteristics of the rocks. The parameters of Young's modulus, Poisson's ratio, density,

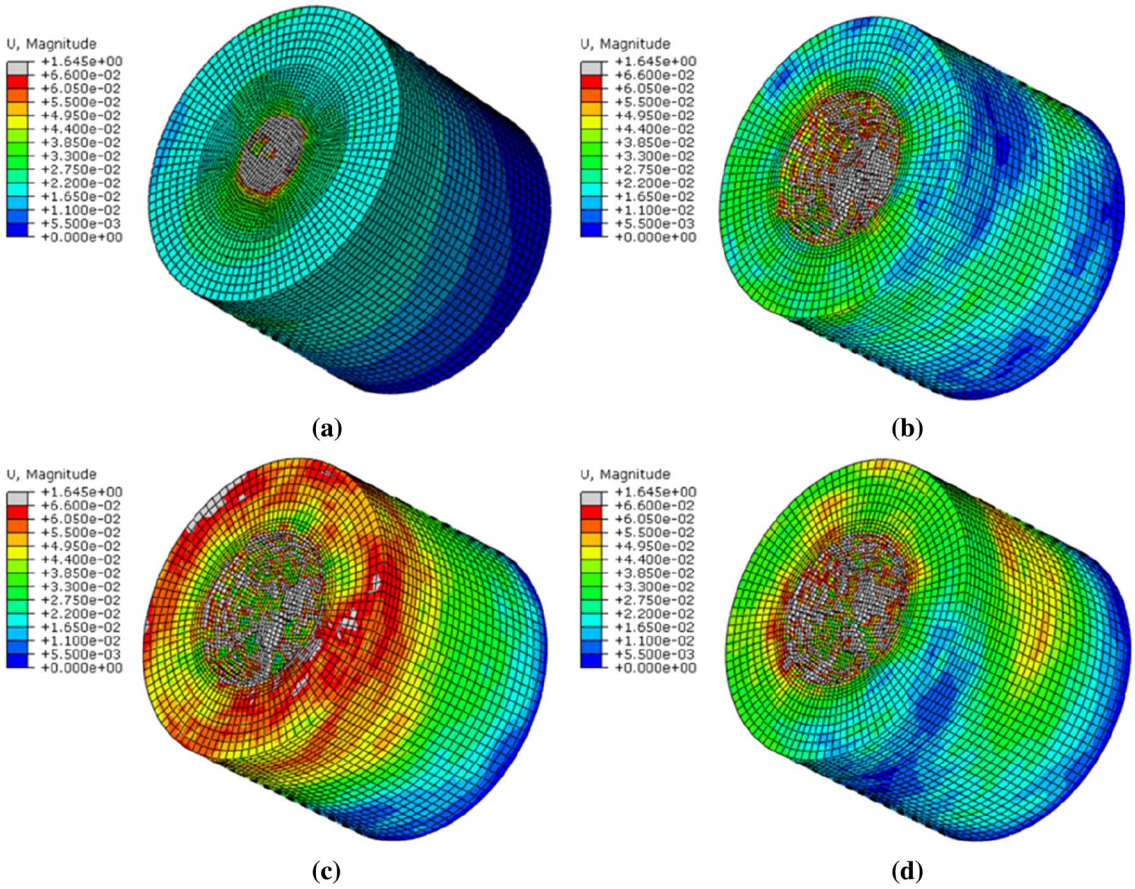

Fig. 11 Distribution of the vibration displacement of rocks of the four lithologies: **a** limestone; **b** sandstone; **c** coal; and **d** mudstone

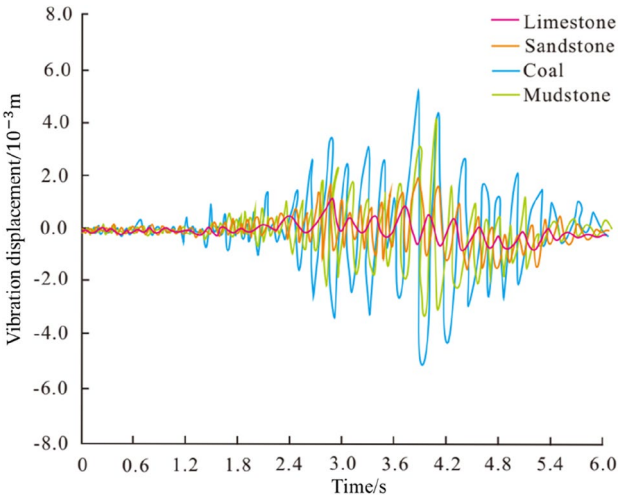

Fig. 12 Variation of the vibration displacement of rocks of the four lithologies

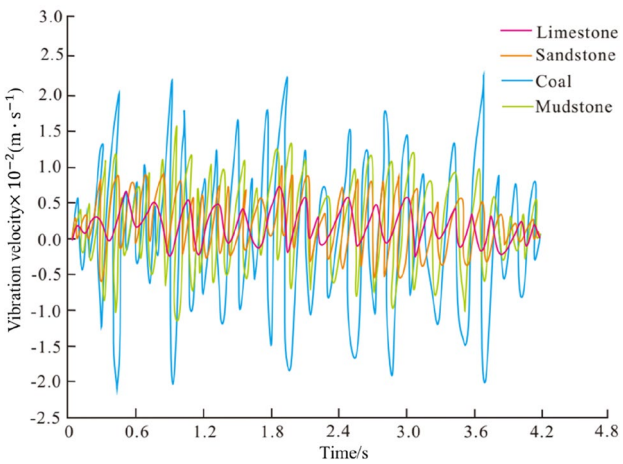

Fig. 13 Vibration velocity of rocks of the four lithologies

compressive strength, and inherent frequency were derived from actual measurements of the coal formation rock via testing in the laboratory, as shown in Table 5.

Relationship between uniaxial compressive strength (σ_c) and vibration response

Rock strength is an important physical parameter that characterizes the mechanical properties of rock and reflects the

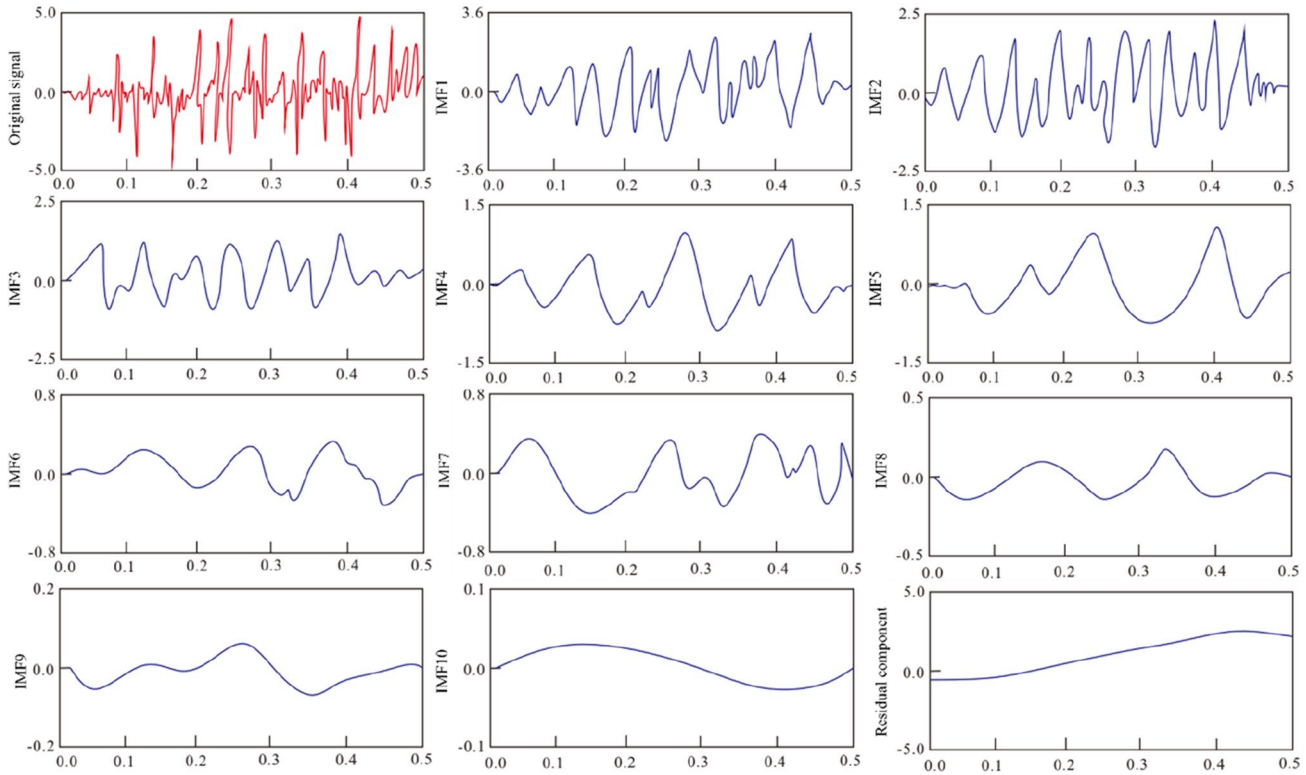

Fig. 14 EMD effect of limestone

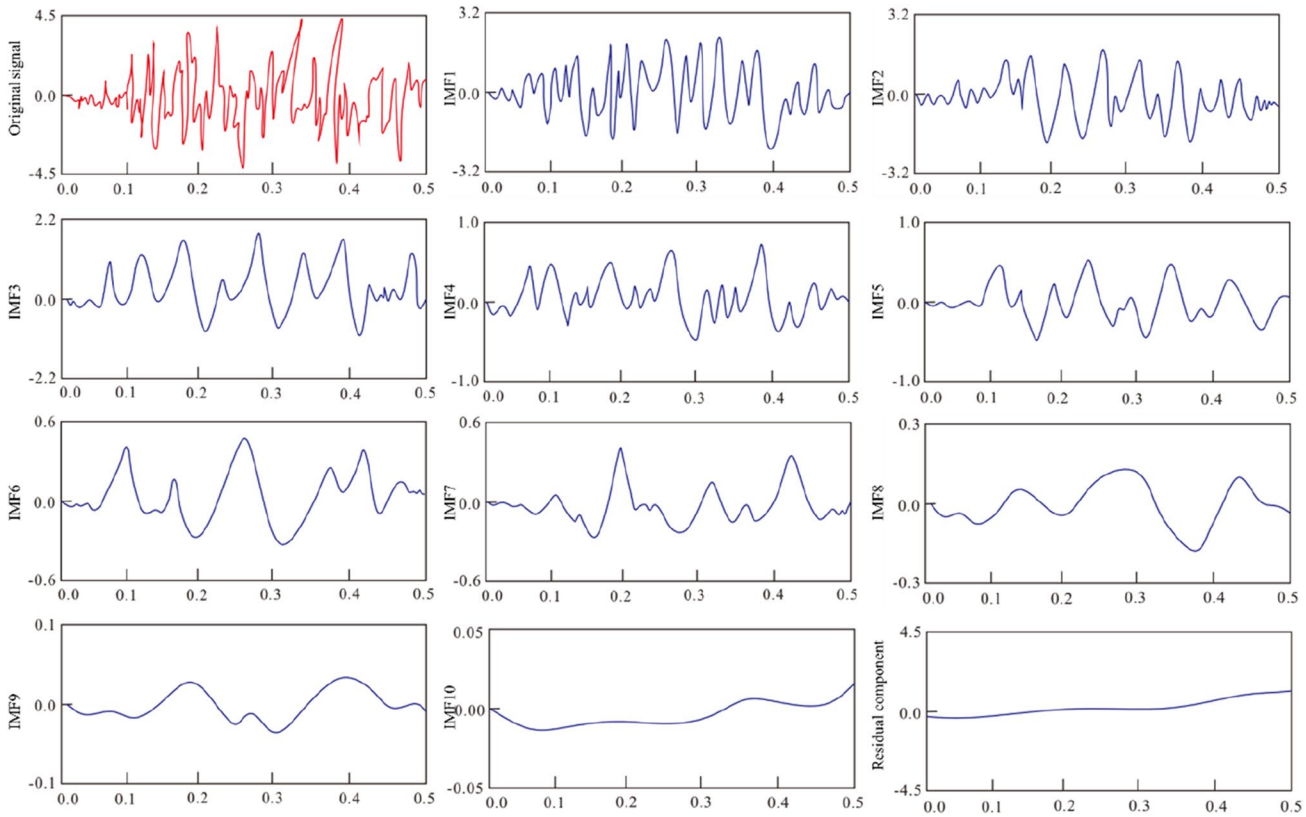

Fig. 15 EMD effect of sandstone

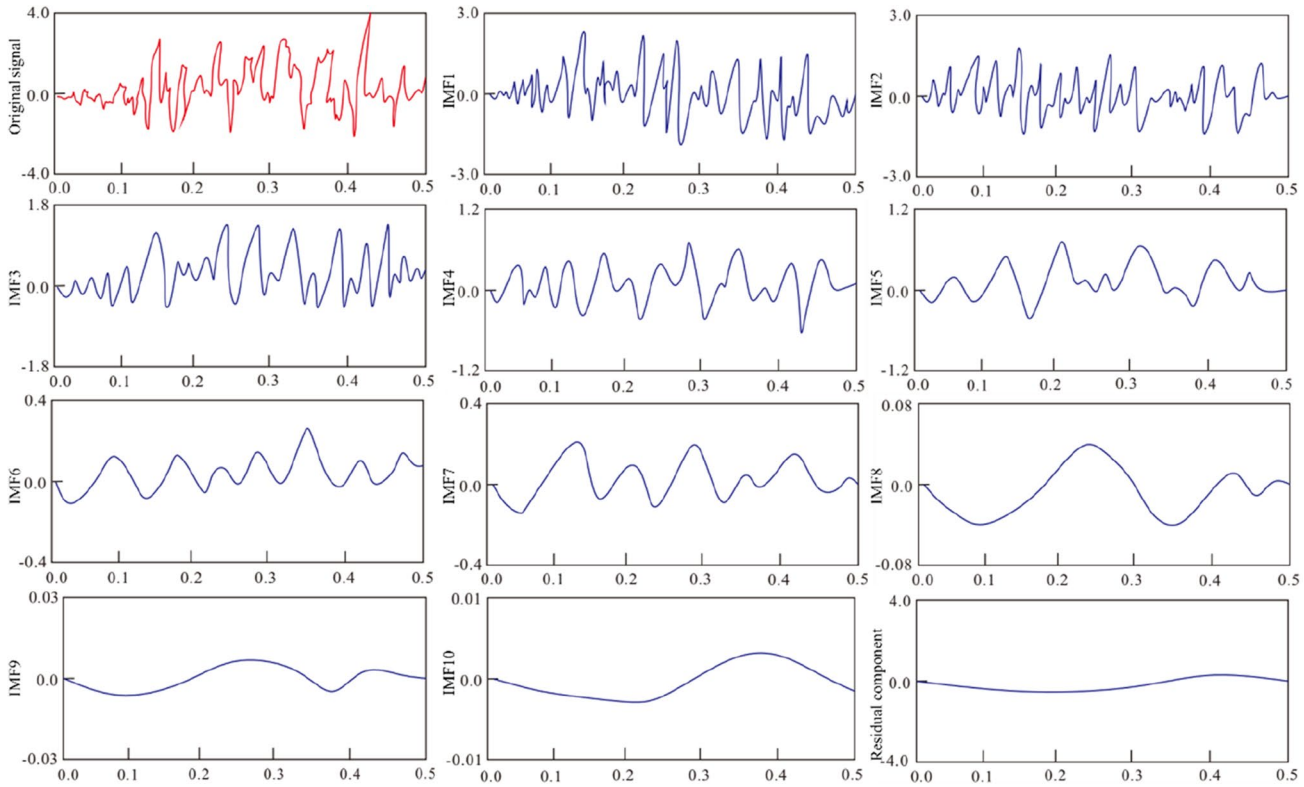

Fig. 16 EMD effect of coal

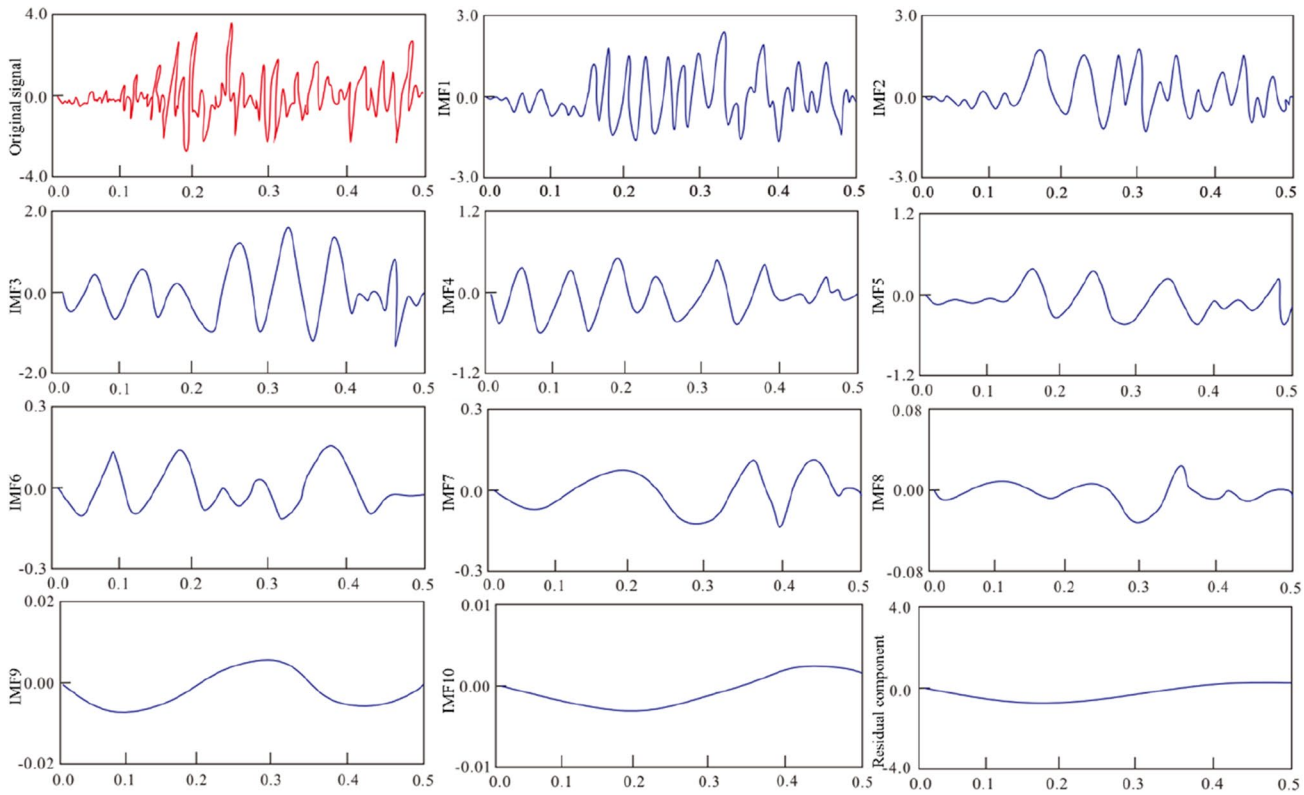

Fig. 17 EMD effect of mudstone

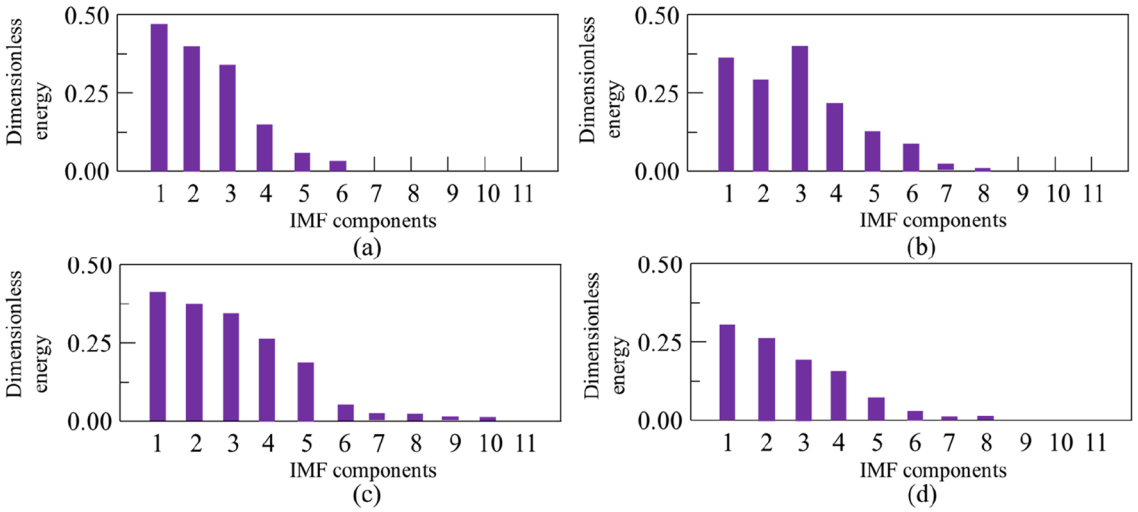

Fig. 18 Dimensionless energy distributions after the EMD decomposition of the four lithologies: **a** limestone; **b** sandstone; **c** coal; and **d** mudstone

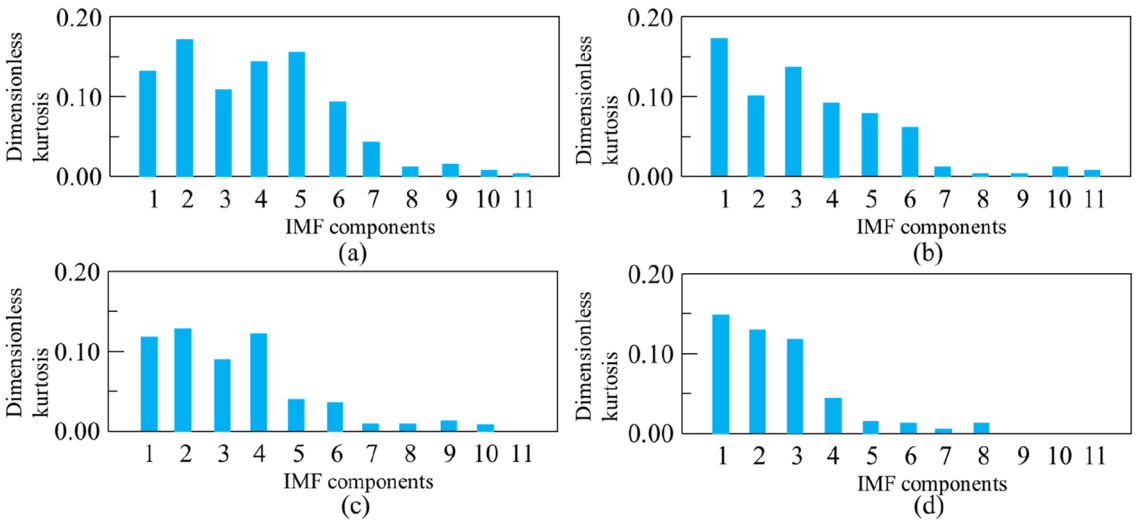

Fig. 19 Dimensionless kurtosis distributions after the EMD decomposition of the four lithologies: **a** limestone; **b** sandstone; **c** coal; and **d** mudstone

ability of rock to resist failure or yield under an external load. It includes uniaxial and triaxial compressive and shear strengths, which mainly distinguished by the different forces involved. The strength characteristics of rock principally depend on the mineral composition, particle size, internal arrangement, internal discontinuity and continuity surfaces, and porosity. When the bit impacts and cuts the rock, differences in internal rock structure also affect the resultant vibration response. In this study, the influence of confining pressure was not considered in the simulations; instead, we focused on the relationship between the uniaxial compressive strength and vibration response. The vibration displacement distribution diagram corresponding to different compressive strengths at the same time ($t = 2.6$ s) is shown in Fig. 21. Vibration displacements differed to some extent under constant WOB, drilling speed, and rotation speed. Lower compressive strength was correlated with greater vibration displacement. At σ_c = 30 MPa, almost all rocks especially vibrated near the bit, the vibration displacement was the largest at this value. Higher compressive strength resulted in smaller and more subtle corresponding vibration displacement. The main reason for this phenomenon was a positive correlation not only between uniaxial compressive strength and critical pressure required to for damage by external impact but also between ease of deformation and magnitude of the vibration effect. However, a greater

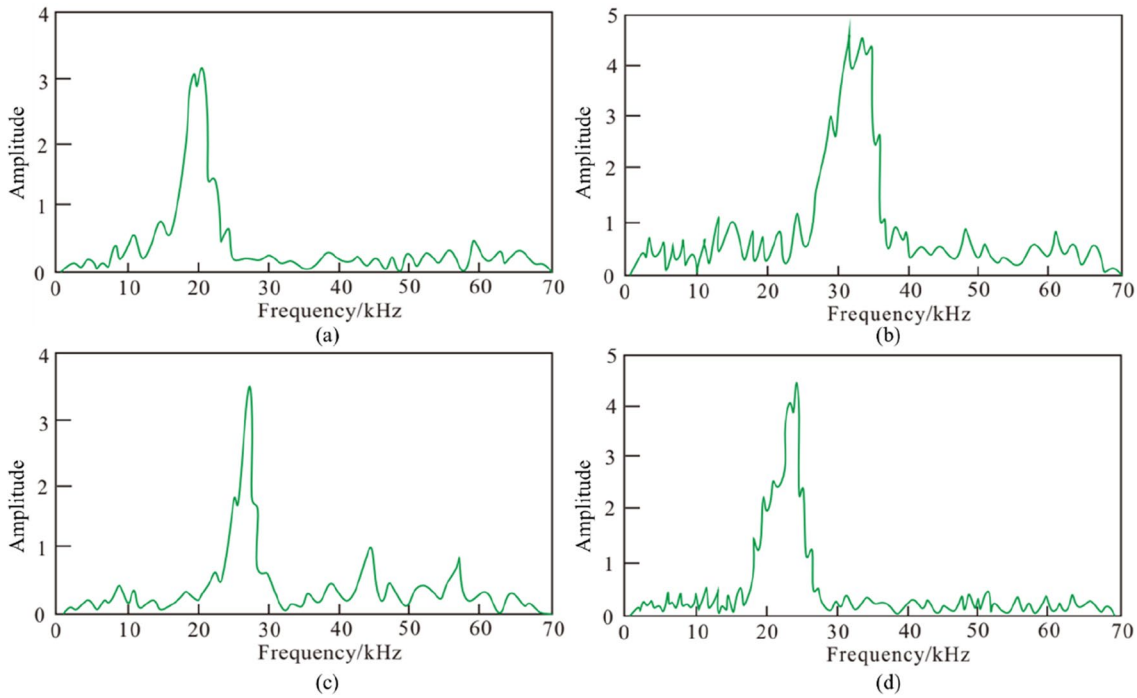

Fig. 20 Distributions of Hilbert marginal spectrum of the four lithologies: **a** mudstone; **b** sandstone; **c** coal; and **d** limestone

Table 4 Peak frequency distribution of the four lithologies

Number	Lithology	Main frequency band (kHz)	Peak frequency (kHz)
1	Limestone	15.6–21.3	19.6
2	Sandstone	20.5–26.3	23.9
3	Coal	23.6–30.3	28.8
4	Mudstone	28.1–34.6	33.4

compressive strength of the rock also corresponded to greater intergranular cohesive force, making it more difficult for deformation and vibration to occur. The vibration velocity and vibration displacement curves at the same unit node were extracted (Fig. 22a and b). The uniaxial compressive strength of the rock significantly influenced the vibration effect, with a smaller compressive strength corresponding to a greater vibration velocity and vibration displacement. Therefore, the uniaxial compressive strength of the rocks was inversely proportional to the vibration response, which was consistent with the experimental results (Table 5).

Relationship between density (ρ) and vibration response

The distribution of vibration displacements of rocks with different densities at the same time point ($t = 2.6$ s) was extracted (Fig. 23). There were significant density-dependent differences when the three drilling parameters were held constant. Lower rock density corresponded to a larger vibration displacement and more pronounced vibration effect. When the rock is subjected to the impact of a drill, it is more susceptible to vibration. Figure 24 shows the variation trend of the displacement of rocks with different densities over time within the same period, illustrating

Table 5 Test values of rock mechanical parameters in the laboratory

Number	Depth (m)	Lithology	Elastic modulus (Gpa)	Poisson's ratio	Rock drill ability	Inherent frequency (kHz)	Density (g cm^{-3})	Uniaxial compressive strength (Mpa)
1	436.7	Fine sandstone	36.4	0.33	3.8	2.02	2.55	45.3
2	655.9	Grit sandstone	43.8	0.31	5.7	2.16	2.57	46.5
3	821.3	Coal	8.6	0.45	2.3	1.83	1.90	21.9
4	1039.5	Limestone	59.1	0.19	7.6	2.31	2.88	70.3

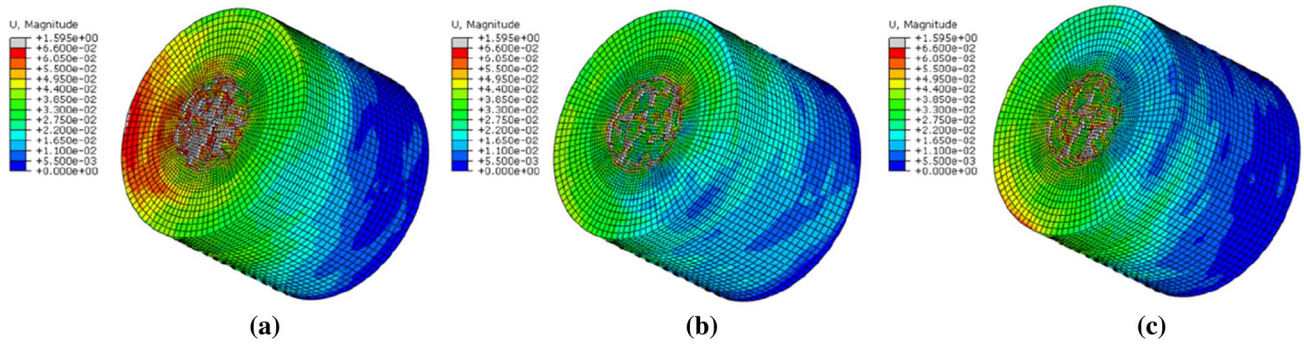

Fig. 21 Vibration displacement distributions of the three uniaxial compressive strengths: **a** σ_c = 30MPa; **b** σ_c = 40MPa; and **c** σ_c = 50MPa

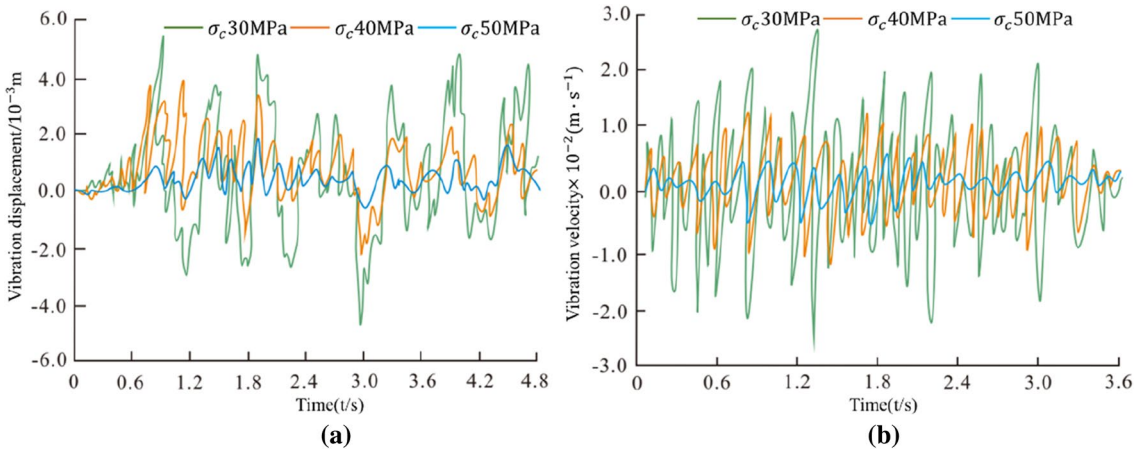

Fig. 22 Variation of **a** vibration displacement and **b** vibration velocity corresponding to the three uniaxial compressive strengths

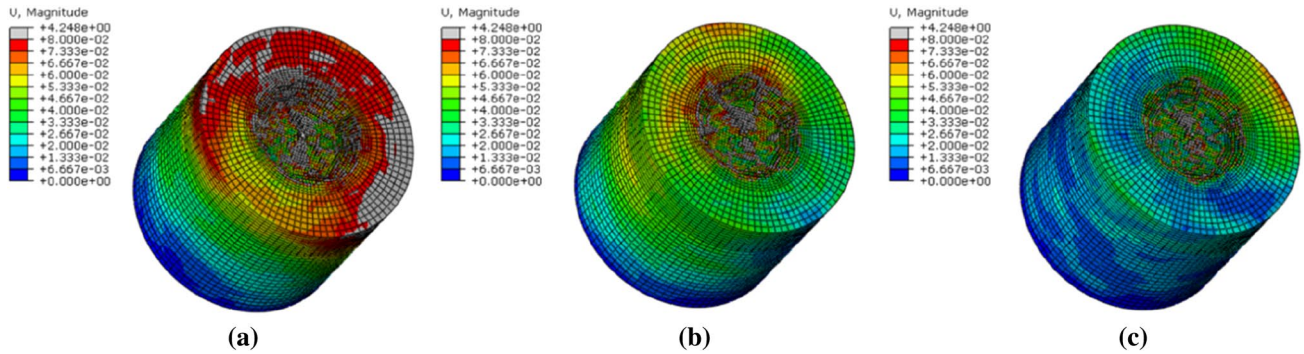

Fig. 23 Vibration displacement distributions of the rocks with the three densities: **a** ρ = 1.8g/cm^3; **b** ρ = 2.3g/cm^3; and **c** ρ = 2.8g/cm^3

that lower densities resulted in greater vibration displacement amplitudes and vibration velocities. This was mainly caused by higher density corresponding to a more compact arrangement of particles, greater cohesive force, and greater resistance to distortion, thereby resulting in a highly pronounced vibration response under the action of an external load. In contrast, a lower density corresponded to a smaller cohesive force and thus lower resistance to particle misalignment, greater ease of deformation, and more pronounced vibration response. Therefore, rock density was inversely proportional to the vibration response, which was consistent with the results of the laboratory experiments (Table 5).

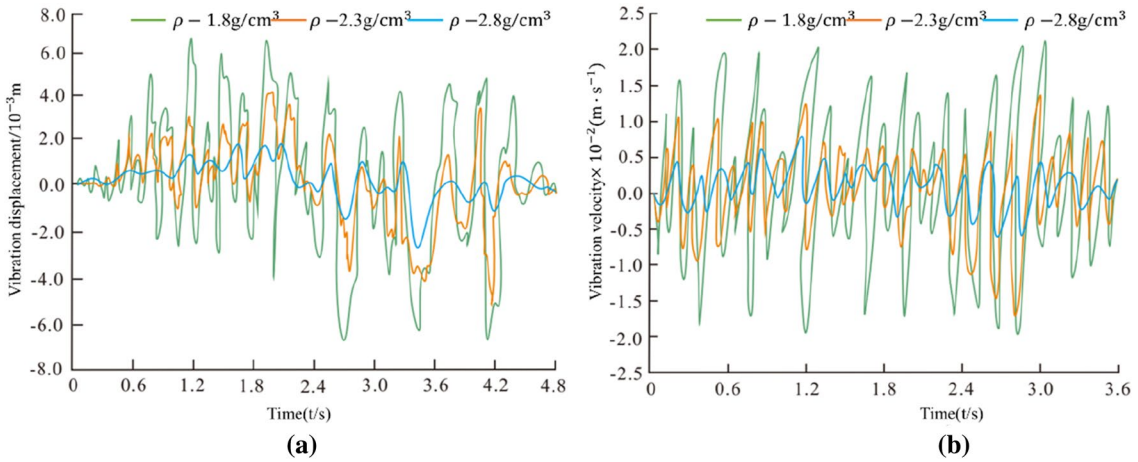

Fig. 24 Variation of **a** vibration displacement and **b** vibration velocity with time for the rocks with the three densities

Relationship between elastic modulus (E) and vibration response

A rock's Young's modulus indicates its ability to resist deformation caused by external load, with larger values corresponding to lower likelihood of deformation. The Young's modulus of a rock is proportional to its hardness. The vibration displacement distribution for the experimental rocks was extracted under constant drilling parameters (Fig. 25), showing that Young's modulus was negatively correlated with vibration displacement. The variation curves of the vibration displacement and vibration velocity at the same element node under different Young's moduli were extracted (Fig. 26). It was confirmed that a larger Young's modulus corresponded to a less pronounced vibration effect, smaller vibration displacement, and lower vibration velocity. This was mainly because rock with a larger Young's modulus was more difficult to deform under an external impact, leading to lower vibration intensity and a less pronounced vibration response. Therefore, it was verified that the vibration response was inversely proportional to the increased Young's modulus, consistent with the results shown in Table 5.

Conclusions

In this study, we used theoretical derivations and numerical simulations to quantify the drilling-vibration response characteristics of rocks of four different lithologies (limestone, sandstone, coal, and mudstone). The following points represent the main conclusions.

1. Stress concentration occurred when the bit interacted with the rock and varied with lithology. Substantial differences in vibration response were observed among the four lithologies. The stress concentration and vibration response in limestone were the greatest, and those in mudstone were the lowest.
2. The drilling-vibration responses of the rocks were closely related to their mechanical properties. The

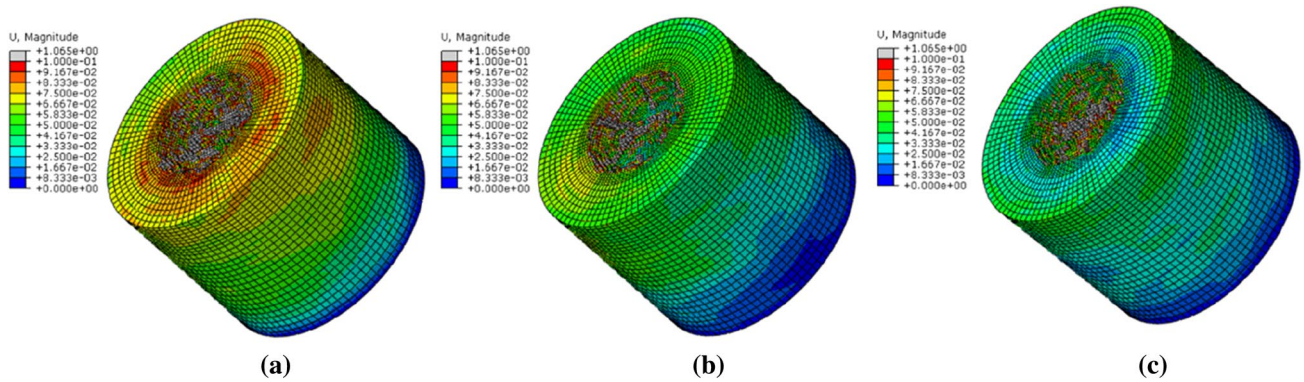

Fig. 25 Vibration displacement distributions of the rocks with the three Young's modulus: **a** $E=9$ GPa; **b** $E=20$ GPa; and **c** $E=50$ GPa

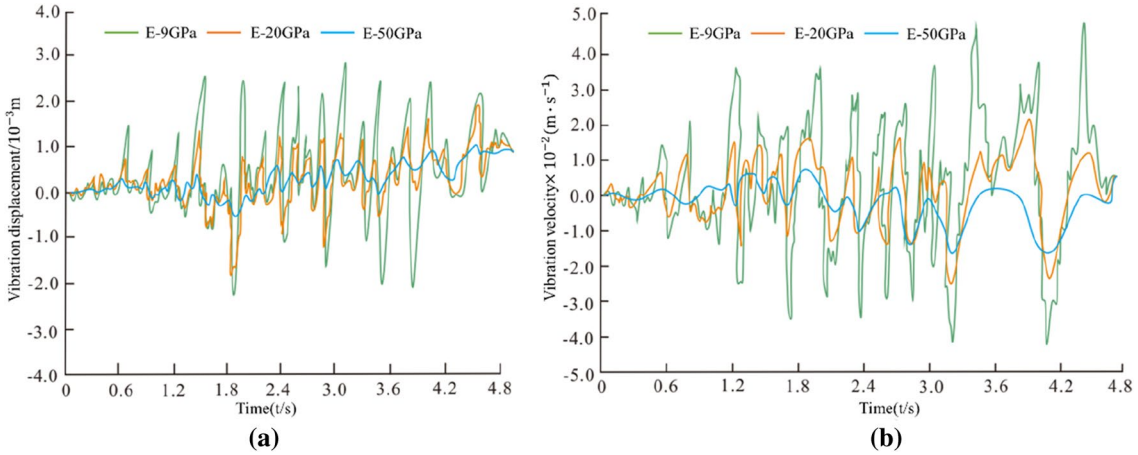

Fig. 26 Variation of **a** vibration displacement and **b** vibration velocity of the rocks with the three Young's modulus

compressive strength, density, and Young's modulus of the rocks influenced their vibration responses. Under constant drilling parameters, the vibration velocity and vibration displacement were inversely proportional to the compressive strength, density, and Young's modulus, and the vibration acceleration was proportional to the Young's modulus.

3. Based on numerical simulation and HHT analysis, substantial differences among different lithologies existed in the vibration velocity, acceleration, and frequency, which provides a reference and methodology for identifying lithologies from drilling data and identifying rock strength characteristics for the adjustment of the drilling parameters.

Acknowledgements I am grateful for the suggestions regarding revision of the numerical simulation proposed by Yunhong Wang, as well as language revision and figure suggestions proposed by Xiao Liu, Xiaoyu Liu, Sihui Xu, Yanqiu Wang, and Xiaowei Ni.

Funding This study was supported by the National Natural Science Fund of China (51974332), Key Basic Research Program of Natural Science of Shannxi Province [2022JZ-16], Key Top-level Design Program of the Major Project of Science and Technology Innovation, and Entrepreneurship Foundation of Tiandi Technology Co., LTD [2020-TD-ZD003], and Development of Large Penetrating Distance Transient Electromagnetic Detection Equipment with Wide Face Grant [2022–2-TD-MS006].

Data availability The datasets generated and analyzed during the present study are not publicly available because of applicable institutional guidelines but are available from the corresponding author upon reasonable request.

Declarations

Conflict of interest All authors declare no conflict of interest.

References

Ahmed A, Elkatatny S, Gamal H et al (2022) Artificial intelligence models for real-time bulk density prediction of vertical complex lithology using the drilling parameters. Arab J Sci Eng 47:10993–11006. https://doi.org/10.1007/s13369-021-05537-3

Aydin SM, Hanifi C (2021) Empirical performance prediction for raise boring machines based on rock properties, pilot hole drilling data and raise inclination. Rock Mech Rock Eng 54:1707–1730. https://doi.org/10.1007/s00603-020-02355-1

Bameri A, Seifabad MC, Hoseinie SH (2021) Laboratorial studies for the prediction of rock texture and hardness using vibration measurement while drilling. Bull Eng Geol Environ 80:8311–8318

Darwesh AK, Rasmussen TM, Al-Ansari N (2020) Controllable drilling parameter optimization for roller cone and polycrystalline diamond bits. J Pet Explor Prod Technol 10:1657–1674. https://doi.org/10.1007/s13202-019-00823-1

Diao YS, Jia DT, Liu GD et al (2022) Structural damage identification using modified Hilbert-Huang transform and support vector machine. J Civ Struct Heal Monit 11:1155–1174. https://doi.org/10.1007/s13349-021-00509-5

Dushyanth ND, Suma MN, Mrityanjaya VL (2016) Detection and localization of damage using empirical mode decomposition and multilevel support vector machine. Appl Phys A Mater Sci Process 122:250

Esmaeili A, Elahifar B, Fruhwirth RK et al (2012) Experimental evaluation of real-time mechanical formation classification using drill string vibration measurements. SPE. https://doi.org/10.2118/158933-MS

Fang XX, Feng H (2021) Study on discriminant method of rock type for porous carbonate reservoirs based on Bayesian theory. Sci Rep 11:18622. https://doi.org/10.1038/s41598-021-98154-x

Fang XX, Feng H, Wang H (2022) Study on intelligent prediction method of rock drillability based on Bayesian lithology classification and optimized BP neural network. Pet Sci Technol 40:2141–2162

Fang XX, Zhu GT, Yang YM et al (2023a) Quantitative method of classification and discrimination of a porous carbonate reservoir integrating K-means clustering and Bayesian theory. Acta Geol Sin Eng Edn 97:176–189. https://doi.org/10.1111/1755-6724.14941

Fang XX, Feng H, Zhang Z et al (2023b) Brittleness index prediction method of tight reservoir based on grey correlation and analytic hierarchical process. Pet Sci Technol 3:1–18. https://doi.org/10.1080/10916466.2023.2172431

Guo SY, Ma NJ (2016) Strata fracturing state and vibration response characteristics of drill. Journal of Mining & Safety Engineering 33:911–917

Jeroen VE, Joan F, David S et al (2021) Rock support prediction based on measurement while drilling technology. Bull Eng Geol Env 80:1449–1465. https://doi.org/10.1007/s10064-020-01957-x

Kenneth OA, Yang L, Evangelos P (2022) Machine learning-based rock characterization models for rotary-percussive drilling. Nonlinear Dyn 109:2525–2545. https://doi.org/10.1007/s11071-022-07565-6

Lakshminarayana CR, Tripathi AK, Pal SK (2020) Prediction of mechanical properties of sedimentary type rocks using rotary drilling parameters. Geotech Geol Eng 38:4863–4876. https://doi.org/10.1007/s10706-020-01332-3

Lee KS, Kim YW, Koo MH et al (2010) Hilbert-Huang Transform (HHT) transient analysis of composite panel undergoing high-velocity impact. J Mech Sci Technol 24:2395–2400

Li CH, Wang CJ, Chen T et al (2011) Determining method for downhole drill string movement station by using drill string vibration frequency spectrum. J China Univ Petr (edition of Natural Science) 5:56–60

Liu G, Zhang JL, Liu C et al (2017) An identification method of vibration signal features when bit drills different mediums. J Vib Shock 8:71–78

Liu SW, Fu MX, Zhang H et al (2016) Vibration mechanism and characteristics analysis of drill rod when drilling roof bolt hole. J China Univ Min Technol 45:893–901

Liu YX, Gao MS, Zhao HS et al (2020) Detection of overlying rock structure and identification of key stratum by drilling and logging technology. J Min Strata Control Eng 2:023038

Majeed Y, Abu Bakar MZ, Butt IA (2020) Abrasivity evaluation for wear prediction of button drill bits using geotechnical rock properties. Bull Eng Geol Env 79:767–787. https://doi.org/10.1007/s10064-019-01587-y

Mehrbod K, Raheb B (2020) Predicting the geomechanical properties of hard rocks using analysis of the acoustic and vibration signals during the drilling process. Geotechn Geol Eng 39:2087–2099

Rajesh BK, Harsha V, Govindaraj M (2011) Prediction of uniaxial compressive strength, tensile strength and porosity of sedimentary rocks using sound level produced during rotary drilling. Rock Mech Rock Eng 44:613–620

Rajesh BK, Harsha V, Govindaraj M et al (2013) Regression analysis and ANN models to predict rock properties from sound levels produced during drilling. Int J Rock Mech Min Sci 58:61–72. https://doi.org/10.1016/j.ijrmms.2012.10.002

Sahoo S, Jha MK (2017) Pattern recognition in lithology classification: modeling using neural networks, self-organizing maps, and genetic algorithms. Hydrogeol J 25:311–330. https://doi.org/10.1007/s10040-016-1478-8

Utku S, Hamit A, Olgay Y (2021) Investigation of the rock drilling performance of rotary core drilling. Bull Eng Geol Env 81:24. https://doi.org/10.1007/s10064-021-02534-6

Vardhan H, Adhikari GR, Govindaraj Raj M (2009) Estimating rock properties using sound level during drilling. Int J Rock Mech Min Sci 46:604–612. https://doi.org/10.1016/j.ijrmms.2008.07.011

Vijaya CK, Harsha V, Murthy CSN (2019) Quantification of rock properties using frequency analysis during core drilling operations. J Inst Eng India Ser D 100:67–81. https://doi.org/10.1007/s40033-019-00174-5

Wang XF, Hu SB, Wang EY et al (2022) Extraction of vibration waveform characteristics of dry ice powder pneumatic rock breaking using Hilbert-Huang transform. Arab J Geosci 15:71. https://doi.org/10.1007/s12517-021-09236-z

Yue ZW, Yue XL, Wang X et al (2022) Experimental study on identification of layered rock mass interface along the borehole while drilling. Bull Eng Geol Environ 81:353. https://doi.org/10.1007/s10064-022-02861-2

Zhu LY, Li ZH, Xu LM (2014) Measuring stress and strength of coal by drilling cutting torque method. Chin J Geotechn Eng 36:2096–2103

Zhu MB, Xie G, Liu L et al (2023) Strengthening mechanism of granulated blast-furnace slag on the uniaxial compressive strength of modified magnesium slag-based cemented backfilling material. Process Saf Environ Prot 174:722–733